Journal of Power Sources 217 (2012) 316–321

Contents lists available at SciVerse ScienceDirect

Journal of Power Sources

journal homepage: www.elsevier.com/locate/jpowsour

Influence of trivalent Gd and Dy codoping on the structure and electrical conductivity of pyrochlore-type $Sm_2Zr_2O_7$

Xiao-Liang Xia [a,b], Zhan-Guo Liu [a], Jia-Hu Ouyang [a,*], Yi Zheng [b]

[a] Institute for Advanced Ceramics, School of Materials Science and Engineering, Harbin Institute of Technology, Harbin 150001, China
[b] Shandong Provincial Key Laboratory of Ocean Environment Monitoring Technology, Shandong Academy of Sciences Institute of Oceanographic Instrumentation, 28 Zhejiang Road, Qingdao 266001, China

HIGHLIGHTS

- Phase transition from fluorite to pyrochlore occurs in $SmDy_{1-x}Gd_xZr_2O_7$ ceramics.
- Electrical conductivity of $Sm_2Zr_2O_7$ is significantly improved by codoping strategy.
- The grain conductivity of $SmGdZr_2O_7$ ceramic is 1.90×10^{-2} S cm^{-1} at 1173 K.
- $SmDy_{1-x}Gd_xZr_2O_7$ ceramics are purely oxide-ion conductors in test temperature range.

ARTICLE INFO

Article history:
Received 28 April 2012
Received in revised form
7 June 2012
Accepted 8 June 2012
Available online 16 June 2012

Keywords:
Codoping
Solid electrolyte
Electrical conductivity
Impedance spectroscopy

ABSTRACT

$SmDy_{1-x}Gd_xZr_2O_7$ ($0 \le x \le 1.0$) ceramics are prepared by solid state reaction method at 1973 K for 10 h in air. The crystal structure and microstructure of $SmDy_{1-x}Gd_xZr_2O_7$ ceramics are investigated by X-ray diffraction (XRD) and scanning electron microscopy (SEM). All the $SmDy_{1-x}Gd_xZr_2O_7$ ceramics ($x = 0.2$, 0.4, 0.6, 0.8, 1.0) exhibit a pyrochlore structure except for $SmDyZr_2O_7$ ceramic. $SmDyZr_2O_7$ ceramic has a defective fluorite structure. The incorporation of Gd^{3+} facilitates a structural evolution from a defective fluorite into an ordered pyrochlore-type structure. Electrical conductivity of $SmDy_{1-x}Gd_xZr_2O_7$ ceramics has been investigated by impedance spectroscopy over a frequency range of 1 Hz to 8 MHz from 673 to 1173 K. The grain conductivity of $SmDy_{1-x}Gd_xZr_2O_7$ ceramics follows the Arrhenius behavior. The grain conductivity of $SmDy_{1-x}Gd_xZr_2O_7$ ceramics increases obviously with increasing Gd^{3+} content in the temperature range of 673–1073 K, and the optimal grain conductivity value is 1.90×10^{-2} S cm^{-1} in the composition of $SmGdZr_2O_7$ ceramic at 1173 K. All the $SmDy_{1-x}Gd_xZr_2O_7$ ceramics are purely oxide ionic conductors in the test temperature range.

1. Introduction

As one of the electrochemical energy conversion devices, solid oxide fuel cells (SOFCs) have received great attention and developed rapidly in the past decades, since they convert the chemical energy to electrical energy directly by an efficient and environmental-friendly way [1]. The performance of solid electrolyte in the SOFCs is of great importance for the development of a low- or intermediate-temperature system. Traditionally, 8 mol.% yttria-stabilized zirconia (8YSZ) is the most common oxide-ion electrolyte for SOFCs, which is usually operated in the high temperature range (generally, 1073–1273 K) to get the required conductivity and high power output [2,3]. However, high operation temperature results in some problems, such as high cost, undesirable interfacial reaction between cathode and electrolyte, which limits the selection of compatible electrode and interconnect materials [4]. Lowering the operating temperature of SOFCs could make SOFCs economically competitive with respect to alternative classical systems because it could reduce the cost and elevate the performance stability of the cell. Tremendous efforts have been made on increasing electrical conductivity of solid electrolytes or searching for novel oxide-ion electrolytes [5]. Alternatively, the intermediate-temperature (773–1073 K) SOFCs based on modified pyrochlore-type $A_2Zr_2O_7$ oxide-ion electrolytes have attracted much interest in the past few years since $A_2Zr_2O_7$ oxides have the structure to accommodate oxygen nonstoichiometry [6].

In the family of pyrochlore-type $A_2Zr_2O_7$ oxides, $Gd_2Zr_2O_7$ with different cations has been extensively investigated as potential electrolyte for intermediate temperature SOFCs and verified to possess high conductivity at comparative temperatures [7–14].

* Corresponding author. Tel./fax: +86 451 86414291.
E-mail address: ouyangjh@hit.edu.cn (J.-H. Ouyang).

0378-7753/$ – see front matter © 2012 Elsevier B.V. All rights reserved.
http://dx.doi.org/10.1016/j.jpowsour.2012.06.034

Electrical conductivity of the pyrochlore-type $Sm_2Zr_2O_7$ was comparable to those of other good oxide-ion conductors in relatively low temperature regions [15]. Although the effect of cation substitution at the Sm site in pyrochlore-type $Sm_2Zr_2O_7$ on the improvement of electrical conductivity was investigated in several literatures [16–18], there are only a few reports concerning electrical behavior when the codopant substitution influence of *A* site near the phase boundary between pyrochlore and fluorite-type phases among the stoichiometric $A_2Zr_2O_7$-type oxides. In order to increase electrical conductivity of solid electrolytes, the co-doping approach has been widely employed and confirmed to be an effective method [19,20]. $Sm_2Zr_2O_7$ co-doped with Gd and Yb cations shows a higher electrical conductivity than undoped $Sm_2Zr_2O_7$ in a temperature range of 723–1173 K [21]. However, the crystal structure and electrical conductivity of $SmDy_{1-x}Gd_xZr_2O_7$ ($0 \le x \le 1.0$) ceramics have not been investigated in the open literature. In the present work, $SmDy_{1-x}Gd_xZr_2O_7$ ($0 \le x \le 1.0$) ceramics were prepared for the first time by the solid state reaction method at 1973 K for 10 h in air. The objective of this work is to investigate the influence of Gd and Dy codoping on the structure and electrical conductivity of pyrochlore-type $Sm_2Zr_2O_7$.

2. Experimental procedures

In the present study, $SmDy_{1-x}Gd_xZr_2O_7$ ($0 \le x \le 1.0$) ceramics were prepared by the pressureless sintering process. Sm_2O_3, Gd_2O_3 and Dy_2O_3 powders (Grirem Advanced Materials Co. Ltd., China; purity $\ge$ 99.99%), and ZrO_2 powders (Nanbo Structural Ceramics Co. Ltd., China; purity $\ge$ 99.9%) were selected as raw materials. Prior to weighing, all raw powders were calcined at 1173 K for 2 h to remove any adsorbed CO_2 and H_2O. Details of preparing bulk ceramics can be found in our previous study [22]. The density of as-sintered samples was measured by the Archimedes principle. Phase structures of as-sintered samples were characterized by an X-ray diffractometer (Rigaku D/Max-rB, Japan) with Cu Kα radiation. Continuous scans were used for qualitative phase identification in the 2θ range of 10–70° at a scan rate of 4° min^{-1}, while slow step scans with a step width of 0.02° and a step time of 3-s were carried out on the diffraction peak of $(311)_F/(622)_{Py}$ in the 2θ range of 56–59° to determine the shifts of X-ray diffraction peaks. The lattice parameters were estimated with silicon as the external standard. A scanning electron microscope (FEI Quanta 200F, the Netherlands) was used to observe the morphology of bulk ceramics. Prior to SEM observations, as-sintered samples were carbon-coated for 30 min to obtain enough electrical conductivity.

The electrical conductivity measurements were conducted by an alternating current complex impedance method in a frequency range of 1 Hz to 8 MHz on the impedance analyzer (Solartron 1260, Hampshire, U.K.). Prior to the conductivity measurements, platinum paste was painted as electrodes on both sides of the disc, and then dried and annealed at 1223 K for 2.5 h in air to ensure a good contact with specimens and erase the solvent. The measurements were performed in air in the temperature range from 673 to 1173 K at a heating rate of 5 K min^{-1} with an increment of 50 K, while the dwelling time is 15 min between consecutive measurements. The electrical conductivity was also measured at different oxygen partial pressures, e.g., 1.0×10^{-4} to 1.0 atm. Measurement was performed in a closed tube furnace from 1173 K to 673 K during cooling. The $P(O_2)$ was controlled with a mixture of N_2 and O_2, and was measured with an YSZ oxygen sensor close to specimens.

3. Results and discussion

Fig. 1(a) and (b) shows XRD patterns of $SmDy_{1-x}Gd_xZr_2O_7$ ceramics pressureless-sintered at 1973 K for 10 h in air. Two types

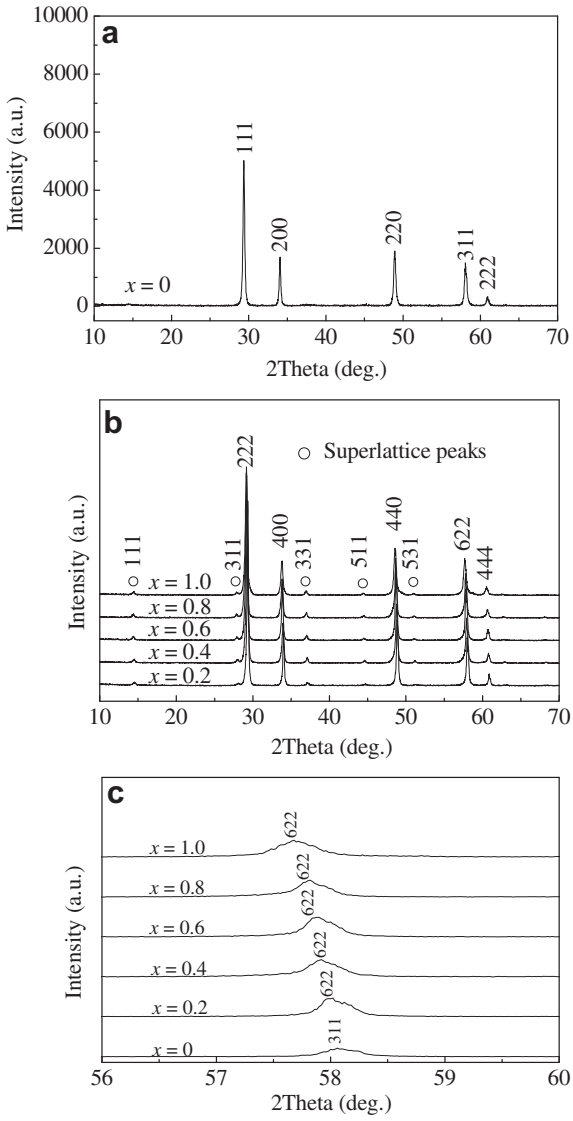

Fig. 1. XRD patterns of $SmDy_{1-x}Gd_xZr_2O_7$ ceramics sintered at 1973 K for 10 h in air: (a) $SmDyZr_2O_7$ ceramic in the 2θ range of 10–70°, (b) $SmDy_{1-x}Gd_xZr_2O_7$ ($0.2 \le x \le 1.0$) ceramics in the 2θ range of 10–70°, (c) $(311)_F/(622)_{Py}$ peak shift in the 2θ range of 56–59°.

of crystal structures appear due to the different composition parameters. It can be seen that $SmDyZr_2O_7$ ($x = 0$) exhibits a disordered defective fluorite structure as shown in Fig. 1(a). With the substitution of smaller Dy^{3+} cations by larger Gd^{3+} cations, $SmDy_{1-x}Gd_xZr_2O_7$ ($x = 0.2, 0.4, 0.6, 0.8, 1.0$) ceramics transform into an ordered pyrochlore-type structure as shown in Fig. 1(b), which is characterized by the presence of superstructure diffraction peaks at $2\theta \approx 14°$ (111), 28° (311), 37° (331), 45° (511) and 51° (531) using Cu Kα radiation [23,24]. In the $A_2Zr_2O_7$ oxides, the crystal structure depends mainly upon the ionic radius ratio of $r(A^{3+})_{average}/r(Zr^{4+})$. The pyrochlore-type structural stability of rare-earth zirconates is located in the range of $1.46 \le r(A^{3+})_{average}/r(Zr^{4+}) \le 1.78$ at an atmospheric pressure. However, if the radius ratio is less than 1.46, a disordered defective fluorite structure is formed. The ionic radius of Sm^{3+}, Gd^{3+} and Dy^{3+} is 1.079 Å, 1.053 Å and 1.027 Å in eight-fold coordination, respectively, while the ionic radius of Zr^{4+} is 0.72 Å in six-fold coordination [25]. $SmDyZr_2O_7$ ceramic with the average ionic radius ratio of $r(Sm^{3+} - Dy^{3+})_{average}/r(Zr^{4+}) = 1.46$ is just located at the boundary of pyrochlore phase region, which has

either pyrochlore-type or defective fluorite-type structure depending on the temperature condition of heat treatment. As the sintering temperature (1973 K) used in this paper is higher than the order–disorder transition temperature (1803 K) of $Gd_2Zr_2O_7$ [26], it is reasonable that $SmDyZr_2O_7$ (just like $Gd_2Zr_2O_7$) has a defective fluorite-type structure as shown in Fig. 1(a). As for other $SmDy_{1-x}Gd_xZr_2O_7$ (x = 0.2, 0.4, 0.6, 0.8, 1.0) ceramics, the pyrochlore-type structure is favored as the average ionic radius ratio of $r(A^{3+})_{average}/r(Zr^{4+})$ is obviously larger than 1.46.

Fig. 1(c) reveals the XRD patterns of $SmDy_{1-x}Gd_xZr_2O_7$ ceramics in the 2θ range of 56–60°. The $(311)_F/(622)_{Py}$ peak of $SmDy_{1-x}Gd_xZr_2O_7$ ceramics shifts gradually to the low angle region with increasing Gd^{3+} content, which is related to the variation in average ionic radius of A site including Sm^{3+}, xGd^{3+} and $(1-x)Dy^{3+}$ cations. The calculated lattice parameters as a function of composition parameter x are presented in Fig. 2, where the lattice parameter of the fluorite phase is doubled for convenience in a comparative study with the pyrochlore phase. An approximately linear increase of the lattice parameters is observed with increasing composition parameter from $x = 0$ to $x = 1.0$, which is in good accordance with the Vegard's rule as [a (nm) = 1.0526 + 0.0061x]. Meanwhile, the increase in the lattice parameter indicates an expansion of the cell volume, which is ascribable to the substitution of larger Gd^{3+} (ionic radius = 0.1053 nm) cations for smaller Dy^{3+} (ionic radius = 0.1027 nm) in the eight-fold coordination.

SEM micrographs of typical sintered $SmDy_{1-x}Gd_xZr_2O_7$ ($0.2 \le x \le 0.8$) ceramics are presented in Fig. 3. Obviously, $SmDy_{1-x}Gd_xZr_2O_7$ ceramics display a dense structure from the surface micrograph; however, there are still some pores at the grain boundary. Although the simple ceramic processing procedure taken in the present work may be not perfect for complete densification, this will not result in any influence on the co-doping effect due to the similarity in density and microstructure for $SmDy_{1-x}Gd_xZr_2O_7$ ceramics. From SEM observations, the average grain size of $SmDy_{1-x}Gd_xZr_2O_7$ ceramics is in the range of 5–10 μm. The grain boundary is clean and no other compounds are observed at the grain boundary, which is in good accordance with the XRD patterns in Fig. 1.

Impedance spectroscopy data collected for the selected sample of $SmDy_{0.2}Gd_{0.8}Zr_2O_7$ at 673 K in air is shown in Fig. 4 in terms of the complex impedance plots of $-Z''$ vs. Z'. It can be seen that there are three contributions in these plots. The high-frequency semicircle is due to the grain polarization; and the intermediate-frequency semicircle and the low-frequency circle are responded to the grain boundary polarization and electrode process, respectively. The contributions of grain resistance and grain-boundary resistance to the total resistance can be resolved by different capacitances or relaxation time in the impedance spectra [20]. In the ideal case, the frequency response of polycrystalline oxide-ion

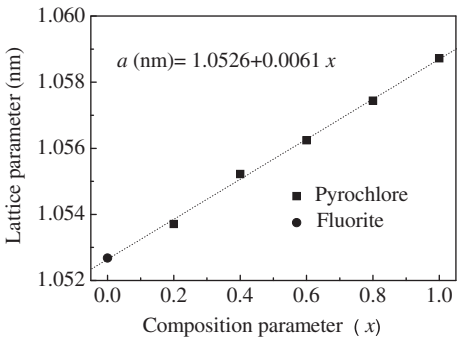

Fig. 2. Lattice parameters of $SmDy_{1-x}Gd_xZr_2O_7$ ceramics.

electrolytes can be modeled by a resistor and a lossy capacitor (RC) in parallel. However, in the present case, taking into account of the microstructure inhomogeneity of the samples, the capacitor has been replaced by a constant phase element (CPE) to fit the experimental data. Therefore, the spectra show somewhat depressed arcs as shown in Fig. 4, The impedance spectra have been modeled by the Z-view software using the configuration of $(R_g//CPE_g)(R_{gb}//CPE_{gb})(R_e//CPE_e)$, where R_g is the grain resistance, R_{gb} is the grain boundary resistance, R_e is the electrode process. The equivalent circuit used is also shown in the complex impedance plots. From the fitted results, the capacitance values obtained for high-frequency and intermediate-frequency circles are 3.85×10^{-11} F cm^{-1} and 2.50×10^{-7} F cm^{-1} for $SmDy_{0.2}Gd_{0.8}Zr_2O_7$ ceramic, which correspond to grain resistance and grain boundary resistance, respectively. Meanwhile, as shown in Fig. 4, the fitted curves can match the measured results, which suggests that the results originated from equivalent circuit are quite reliable and the obtained grain and grain boundary resistance are reasonable. At a given temperature, grain resistance values R_g are determined from the intercepts of high frequency arcs on the Z' axes [27]. Accordingly, electrical conductivity σ_g can be calculated from grain resistance R_g using the following equation:

$$\sigma_g = l/R_g S \quad (1)$$

where R_g is grain resistance, l is the sample thickness, and S is electrode active area of the sample. Accordingly, the electrical conductivity in the measurement temperature range of 673–1173 K can be obtained.

The variations of the grain conductivity with temperature (Arrhenius equation) for all of these compositions over the temperature range of 673–1173 K are shown in Fig. 5. Apparently, the Arrhenius relationship of the grain resistance ($\log \sigma_g \cdot T$) with respect to the reciprocal of temperature ($1000/T$) is linear, which confirms that the migration of oxide ion is a thermally activated process. The activation energy E_g and pre-exponential factor σ_{0g} are calculated from the slopes and the intercepts of the linear fits of the above plots, respectively. The calculated values of activation energy and pre-exponential factor are shown in Fig. 6. It can be seen that the activation energy of grain conduction decreases with a change in the composition from $SmDyZr_2O_7$ (1.10 eV) with increasing Gd^{3+} substitution and is minimum for $SmGdZr_2O_7$ (0.73 eV) (as shown in Fig. 6). Meanwhile, a similar trend is also observed in the variation of the pre-exponential factor with an increase in the Gd^{3+} content. It has been shown that cooperative effect in oxygen hopping dynamics is a key factor in determining the activation energy for long-range ionic transport in similar systems [28–30], and an enhancement in ion–ion interaction leads to a higher degree of cooperativity in the many-ion-hopping process. The more disordered structure promotes ion–ion correlations, and leads to an increase of the energy penalty that these correlations impose on long-range or ionic conductivity [31]. In the present case, $SmDyZr_2O_7$ is a fluorite-type structure with a significant amount of disorder in it, whereas $SmGdZr_2O_7$ is an ordered pyrochlore phase. Obviously, the addition of more and more Gd^{3+} into $SmDyZr_2O_7$ increases the degree of structural order, which causes the reduction in the degree of correlations among mobile oxide ions in the diffusion process. In turn, this results in a decrease in the energy of activation of grain conduction as the structure becomes more ordered. Additionally, in the case of A-site doping, the decrease in activation energy upon ordering has also been interpreted in terms of an increase in the cell volume. It is reported that the cell volume is linearly dependent upon the ionic radius of the A-site cation in $A_2Zr_2O_7$-type compounds [32]. A larger unit cell volume makes it easier for the mobile oxide ions to migrate, and consequently

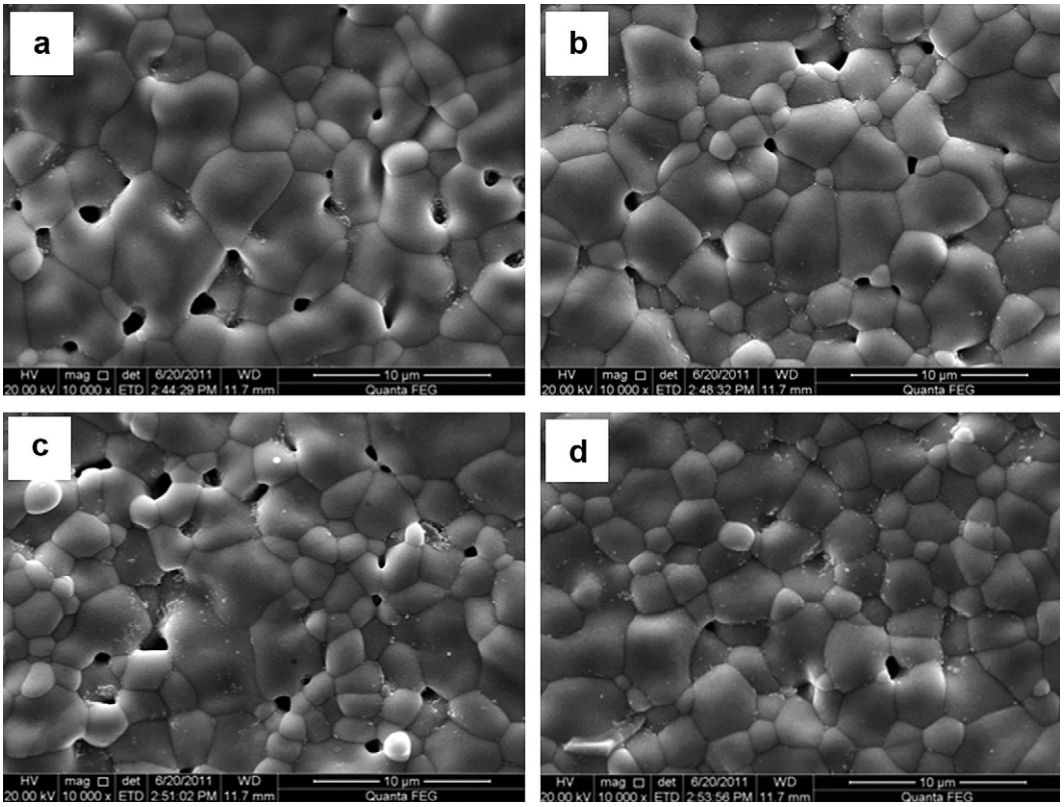

Fig. 3. SEM micrographs of typical $SmDy_{1-x}Gd_xZr_2O_7$ ceramics sintered at 1973 K for 10 h: (a) $x = 0.2$; (b) $x = 0.4$; (c) $x = 0.6$; (d) $x = 0.8$.

a lower energy barrier for mobile oxide ions is expected. The calculations have also been carried out on similar systems, and there are preferential diffusion paths through the cation tetrahedra around the 48*f* oxygen sites in the ordered pyrochlore-type structure and these should lead to a decrease in the strain energy contribution to the activation enthalpy for conductivity, therefore resulting in lower activation energy and higher conductivity upon ordering [33]. A decreasing trend in pre-exponential factor σ_{0g} with an increase in the Gd^{3+} content indicates a decrease in the concentration of mobile oxide ions, which decreases as the degree of structural order increases in the series [34].

Fig. 7 shows grain conductivity of $SmDy_{1-x}Gd_xZr_2O_7$ ceramics as a function of composition parameter at different temperatures. The grain conductivity gradually increases with increasing temperature from 673 to 1173 K for each composition, which also illustrates that the oxide-ion diffusion process in the series is thermally activated. The grain conductivity σ_g increases distinctly with increasing Gd^{3+} content for $0 \leq x \leq 0.6$ in the temperature range of 673–1073 K. With further increasing Gd^{3+} content from $x = 0.6$ to 1.0, the grain conductivity increases slightly and reaches a maximum value at $x = 1.0$ at identical temperature levels. However, the grain conductivity remains almost constant above 1073 K, which indicates that the grain conductivity is independent of the composition at elevated temperatures. Similar results were also found in the $(Gd_{1-x}Eu_x)_2Zr_2O_7$ solid solution [10]. The highest electrical conductivity value in this investigation is 1.90×10^{-2} S cm^{-1} for $SmDy_{1-x}Gd_xZr_2O_7$ ceramics at 1173 K. It should be noted that there is a sharp and almost linear decrease in the activation energy with increasing Gd^{3+} content, although the decrease in the pre-exponential factor is not so significant. Thus, there are two factors that are operating in the series, i.e., a decrease in the available number of mobile oxide ions due to an increase in the structural

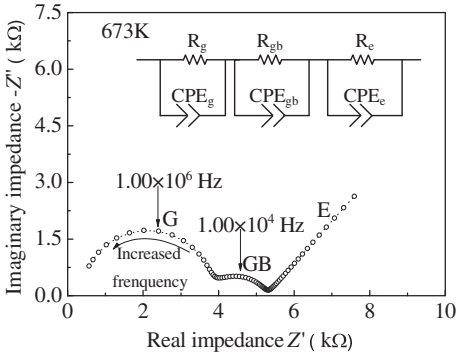

Fig. 4. Complex impedance and corresponding equivalent circuit for $SmDy_{0.2}Gd_{0.8}Zr_2O_7$ ceramic at 673 K in air.

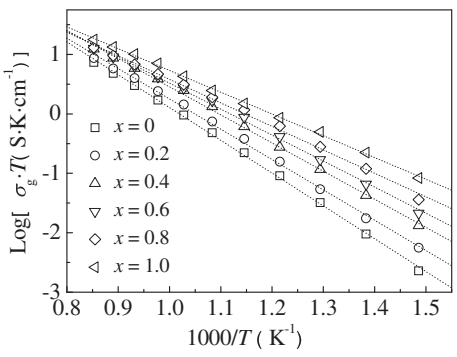

Fig. 5. Arrhenius plots of grain conductivity for $SmDy_{1-x}Gd_xZr_2O_7$ ceramics.

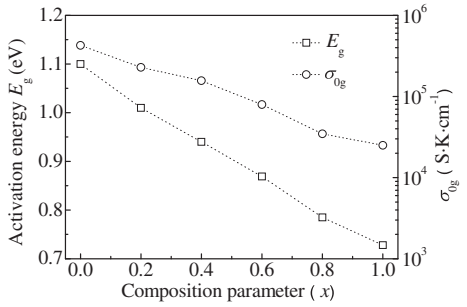

Fig. 6. Activation energy E_g and pre-exponential factor σ_{0g} of grain conductivity for $SmDy_{1-x}Gd_xZr_2O_7$ ceramics as a function of composition.

order and a decrease in resistance imposed on the migration of oxide ions as a consequence of an expansion of the unit cell volume and the reduced interactions among mobile oxide ions as the structural order increases. Both of these factors are competing and control the variations in electrical conductivity. Probably, the increase in electrical conductivity is mainly brought about by an increase in oxide ion mobility rather than a decrease in the available number of mobile charge carriers. Therefore, the measured electrical conductivity of $SmDy_{1-x}Gd_xZr_2O_7$ ceramics increases significantly with increment of Gd^{3+} content in the temperature range of 673–1073 K. In conclusions, the measured electrical conductivity of $Sm_2Zr_2O_7$ ceramics is significantly enhanced by the codoping of Gd^{3+} and Dy^{3+} cations.

The electrical conductivity in a reducing atmosphere was also measured to prove that the conductivity is purely ionic. In the present work, the grain conductivity of $SmDy_{1-x}Gd_xZr_2O_7$ ceramics is investigated in the oxygen partial pressure range, e.g., 1.0×10^{-4} to 1.0 atm from 673 to 1173 K. Fig. 8 shows the grain conductivity of selected $SmDy_{0.2}Gd_{0.8}Zr_2O_7$ ceramic as a function of oxygen partial pressure $P(O_2)$ at different temperatures. Obviously, the grain conductivity of $SmDy_{0.2}Gd_{0.8}Zr_2O_7$ ceramic is almost independent of oxygen partial pressure from 1.0×10^{-4} to 1.0 atm in the temperature range of 673–1173 K, which indicates that the oxide-ion conduction of $SmDy_{0.2}Gd_{0.8}Zr_2O_7$ ceramic is dominated [35]. In consideration of the fact that both the $(Gd_{1-x}Sm_x)_2Zr_2O_7$ and $(Sm_{1-x}Dy_x)_2Zr_2O_7$ solid solutions are oxide-ion conductors [7,18], it can be concluded that the $SmDy_{1-x}Gd_xZr_2O_7$ ceramics are all purely oxide ionic conductors.

In order to compare the electrical properties of co-doped $Sm_2Zr_2O_7$ to those of 8 mol.% Y_2O_3–ZrO_2 (8YSZ), the total conductivity of selected $SmGdZr_2O_7$ ceramic was also calculated from the impedance spectrum. A comparative study of total

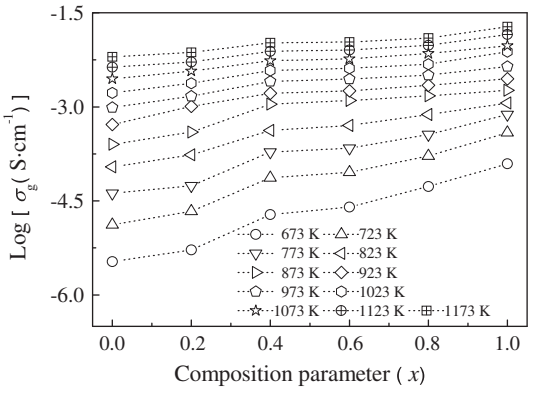

Fig. 7. Grain conductivity of $SmDy_{1-x}Gd_xZr_2O_7$ ceramics as a function of composition.

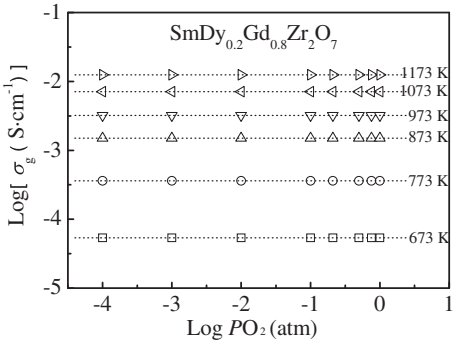

Fig. 8. Oxygen partial pressure dependence of grain conductivity for $SmDy_{0.2}Gd_{0.8}Zr_2O_7$.

Table 1
A comparative study of total conductivity for 8YSZ and $SmGdZr_2O_7$ ceramics.

Total conductivity (S cm^{-1})						
Ceramics	Temperature (K)					
	673	773	873	973	1073	1173
$SmGdZr_2O_7$	9.68E−5	6.77E−4	1.68E−3	4.32E−3	9.30E−3	1.89 E−2
8YSZ [36]	1.77E−4	1.22E−3	5.43E−3	1.50E−2	4.00E−2	8.44 E−2

conductivity for 8YSZ and $SmGdZr_2O_7$ ceramics is shown in Table 1. From Table 1, the total conductivity of $SmGdZr_2O_7$ ceramic is lower than that of 8YSZ electrolyte in the temperature range of 673–1173 K, which indicates that the selected composition is not superior to 8YSZ electrolyte in terms of electrical conductivity. However, when this composition of $SmGdZr_2O_7$ ceramic as SOFCs electrolyte is operated at high temperatures, unexpected chemical reactions between electrolyte and cathode can be suppressed due to their high chemical stability, which is quite different from 8YSZ electrolyte. Taking into account of the electrical conductivity and high chemical stability of these compositions, the most likely applications of $SmDy_{1-x}Gd_xZr_2O_7$ ceramics in high temperature SOFCs are thick-film electrolytes [36].

4. Conclusions

$SmDy_{1-x}Gd_xZr_2O_7$ ($0.2 \leq x \leq 1.0$) ceramics exhibit an ordered pyrochlore structure; however, $SmDyZr_2O_7$ ceramic has a disordered defective fluorite structure. The grain conductivity of $SmDy_{1-x}Gd_xZr_2O_7$ ceramics obeys the Arrhenius equation. Both activation energy and pre-exponential factor for grain conductivity increase with increasing Gd^{3+} content. The grain conductivity of $SmDy_{1-x}Gd_xZr_2O_7$ ceramics increases with increasing Gd^{3+} content in the temperature range of 673–1073 K, and reaches the maximum at 1173 K for all compositions. The highest value in the present work is 1.90×10^{-2} S cm^{-1} at 1173 K for $SmGdZr_2O_7$ ceramic. The $SmDy_{1-x}Gd_xZr_2O_7$ ceramics possess purely ionic conduction with negligible electronic conduction in the test temperature range. The electrical properties of pyrochlore-type $Sm_2Zr_2O_7$ oxide ion electrolytes can be improved by the codoping strategy. However, these compositions are still not superior to 8YSZ electrolyte in terms of electrical conductivity.

Acknowledgments

The authors would like to thank financial support from the National Natural Science Foundation of China (NSFC-Nos. 50972030 and 51021002), and the Fundamental Research Funds for the Central Universities (Grant No. HIT.BRET1.2010006).

References

[1] B.C.H. Steele, A. Heinzel, Nature (London) 414 (2001) 345–352.
[2] J.W. Fergus, J. Power Sources 162 (2006) 30–40.
[3] A.J. Jacobson, Chem. Mater. 22 (2010) 660–674.
[4] D.J.L. Brett, A. Atkinson, N.P. Brandon, S.J. Skinnerd, Chem. Soc. Rev. 37 (2008) 1568–1578.
[5] J. Prado-Gonjal, R. Schmidt, J. Espíndola-Canuto, P. Ramos-Alvarez, E. Morán, J. Power Sources 209 (2012) 163–171.
[6] M.A. Subramanian, G. Aravamudan, G.V. Subba Rao, Prog. Solid State Chem. 15 (1983) 55–143.
[7] Z.-G. Liu, J.-H. Ouyang, Y. Zhou, X.L. Xia, J. Power Sources 185 (2008) 876–880.
[8] J.A. Díaz-Guillén, M.R. Díaz-Guillén, J.M. Almanza, A.F. Fuentes, J. Santamaría, C. León, J. Phys. Condens. Matter 19 (2007) 356212.
[9] J.A. Díaz-Guillén, A.F. Fuentes, M.R. Díaz-Guillén, J.M. Almanza, J. Santamaría, C. León, J. Power Sources 186 (2009) 349–352.
[10] X.-L. Xia, J.-H. Ouyang, Z.-G. Liu, J. Am. Ceram. Soc. 93 (2010) 1074–1080.
[11] B.P. Mandal, S.K. Deshpande, A.K. Tyagi, J. Mater. Res. 23 (2008) 911–916.
[12] B.P. Mandal, A. Dutta, S.K. Desppande, R.N. Basu, A.K. Tyagi, J. Mater. Res. 24 (2009) 2855–2862.
[13] X.-L. Xia, S. Gao, Z.-G. Liu, J.-H. Ouyang, Electrochim. Acta 55 (2010) 5301–5306.
[14] M.R. Díaz-Guillén, K.J. Moreno, J.A. Díaz-Guillén, A.F. Fuentes, K.L. Ngai, J. Garcia-Barriocanal, J. Santamaría, C. León, Phys. Rev. B 78 (2008) 104304.
[15] K. Shinozaki, M. Miyauchi, K. Kuroda, O. Sakurai, N. Mizutani, M. Kato, J. Am. Ceram. Soc. 62 (1979) 538–539.
[16] X.-L. Xia, J.-H. Ouyang, Z.-G. Liu, S. Gao, S. Li, J. Electrochem. Soc. 157 (2010) B470–B476.
[17] Z.-G. Liu, J.-H. Ouyang, Y. Zhou, X.-L. Xia, Electrochim. Acta 54 (2009) 3968–3971.
[18] X.-L. Xia, Z.-G. Liu, J.-H. Ouyang, J. Power Sources 196 (2011) 1840–1846.
[19] B. Li, Y.Y. Liu, X. Wei, W. Pan, J. Power Sources 195 (2010) 969–976.
[20] Z. Gao, X.M. Liu, B. Bergman, Z. Zhao, J. Power Sources 208 (2012) 225–231.
[21] Z.-G. Liu, J.-H. Ouyang, K.N. Sun, X.L. Xia, J. Power Sources 195 (2010) 7225–7229.
[22] X.-L. Xia, J.-H. Ouyang, Z.-G. Liu, J. Power Sources 189 (2009) 888–893.
[23] Z.H. Xu, S.M. He, L.M. He, R.D. Mu, G.H. Huang, X.Q. Cao, J. Alloys Compd. 509 (2011) 4273–4283.
[24] Z.-G. Liu, J.-H. Ouyang, Y. Zhou, J. Li, X.-L. Xia, J. Eur. Ceram. Soc. 29 (2009) 647–652.
[25] R.D. Shannon, Acta Cryst. A32 (1976) 751–767.
[26] D. Michel, M. Perez-y-Jorba, R. Collongues, Mater. Res. Bull. 9 (1974) 1457–1468.
[27] J.R. Macdonald, W.B. Johnson, in: E. Barsoukov, J.R. Macdonald (Eds.), Impedance Spectroscopy: Theory, Experiment and Applications, second ed., John Wiley & Sons, Inc., New Jersey, 2005 (Chapter 1).
[28] K.J. Moreno, G. Mendoza-Suárez, A.F. Fuentes, J. García-Barriocanal, C. León, J. Santamaría, Phys. Rev. B 71 (2005) 132301.
[29] K.J. Moreno, A.F. Fuentes, M. Maczka, J. Hanuza, U. Amador, J. Santamaría, C. León, Phys. Rev. B 75 (2007) 184303.
[30] J. Garcia-Barriocanal, A. Rivera-Calzada, M. Varela, Z. Sefrioui, M.R. Díaz-Guillén, K.J. Moreno, J.A. Díaz-Guillén, E. Iborra, A.F. Fuentes, S.J. Pennycook, C. León, J. Santamaría, Chem. Phys. Chem. 10 (2009) 1003–1011.
[31] J.A. Díaz-Guillén, M.R. Díaz-Guillén, K.P. Padmasree, A.F. Fuentes, J. Santamaría, C. León, Solid State Ionics 179 (2008) 2160–2164.
[32] H. Yamamura, H. Nishino, K. Kakinuma, K. Nomura, Solid State Ionics 158 (2003) 359–365.
[33] A.J. Burggraaf, T. van Dijk, M.J. Verkerk, Solid State Ionics 5 (1981) 519–522.
[34] J. Chen, J. Lian, L.M. Wang, R.C. Ewing, Phys. Rev. Lett. 88 (2002) 105901.
[35] J.B. Goodenough, Annu. Rev. Mater. Res. 33 (2003) 91–128.
[36] V.V. Kharton, F.M.B. Marques, A. Atkinson, Solid State Ionics 174 (2004) 135–149.